Spin-Conservation Propensity Rule for Three-Body Recombination of Ultracold Rb Atoms

Shinsuke Haze, José P. D'Incao, Dominik Dorer, Markus Deiß, Eberhard Tiemann, Paul S. Julienne, and Johannes Hecker Denschlag

Phys. Rev. Lett. **128**, 133401 — Published 1 April 2022

DOI: 10.1103/PhysRevLett.128.133401

Spin-conservation propensity rule for three-body recombination of ultracold Rb atoms

Shinsuke Haze,[1,*] José P. D'Incao,[1,2] Dominik Dorer,[1] Markus Deiß,[1]
Eberhard Tiemann,[3] Paul S. Julienne,[1,4] and Johannes Hecker Denschlag[1,†]

[1]*Institut für Quantenmaterie and Center for Integrated Quantum Science and Technology IQST, Universität Ulm, D-89069 Ulm, Germany*
[2]*JILA, NIST and Department of Physics, University of Colorado, Boulder, CO 80309-0440, USA*
[3]*Institut für Quantenoptik, Leibniz Universität Hannover, 30167 Hannover, Germany*
[4]*Joint Quantum Institute, University of Maryland and NIST, College Park, MD 20742, USA*

(Dated: February 23, 2022)

We explore the physical origin and the general validity of a propensity rule for the conservation of the hyperfine spin state in three-body recombination. This rule was recently discovered for the special case of ^{87}Rb with its nearly equal singlet and triplet scattering lengths. Here, we test the propensity rule for ^{85}Rb for which the scattering properties are very different from ^{87}Rb. The Rb_2 molecular product distribution is mapped out in a state-to-state fashion using REMPI detection schemes which fully cover all possible molecular spin states. Interestingly, for the experimentally investigated range of binding energies from zero to $\sim 13\,\mathrm{GHz}\times h$ we observe that the spin-conservation propensity rule also holds for ^{85}Rb. From these observations and a theoretical analysis we derive an understanding for the conservation of the hyperfine spin state. We identify several criteria to judge whether the propensity rule will also hold for other elements and collision channels.

The particular mechanisms of chemical reactions often give rise to selection and propensity rules. While selection rules express strict exclusion principles for product channels, propensity rules specify which product channels are more likely to be populated than others [1, 2]. Since the early days of quantum mechanics a central question in reaction dynamics is whether composite spins are conserved. Wigner's spin-conservation rule, e.g., states that the total electronic spin has a propensity to be conserved [3–5]. The recent progress in the quantum state-resolved preparation and detection of ultracold atoms and molecules has now made it possible to experimentally explore spin conservation rules that also involve nuclear spins. In a recent study of bimolecular reactions of ultracold KRb molecules the conservation of the total nuclear spin was found [6, 7]. In a study on the final state distribution of three-body recombination of ultracold ^{87}Rb atoms our group found a propensity for the conservation of the hyperfine state of the atom pair forming the molecule [8, 9]. More precisely, this spin propensity rule states that the angular momentum quantum numbers F, f_a, f_b and $m_F = m_{fa} + m_{fb}$ are conserved in the reaction. Here, f_a, f_b correspond to the total angular momenta of the two atoms (a, b) forming the molecule, and $\vec{F} = \vec{f}_a + \vec{f}_b$.

Formally, there is no selection rule that forbids spin exchange between all three atoms in the recombination process, and a corresponding change in the quantum numbers. In fact, recent calculations predict spin exchange to occur in three-body recombination of ^{7}Li [10] and ^{39}K [11, 12], although being suppressed for ^{87}Rb [10]. In order to explain the observed spin propensity rule for ^{87}Rb one can justifiably argue that ^{87}Rb is special since here the singlet (a_s) and triplet (a_t) scattering lengths are nearly identical ($a_s \approx 90a_0, a_t \approx 99a_0$, where a_0 is the Bohr radius). This leads to a strong suppression of two-atom spin exchange reactions [13–15].

In order to explore the validity of the spin propensity rule further, we investigate here, both experimentally and theoretically, three-body recombination of ultracold ^{85}Rb atoms which have very different two-body scattering properties from ^{87}Rb atoms. The singlet and triplet scattering lengths for ^{85}Rb atoms are $a_s = 2720a_0$ and $a_t = -386.9a_0$ [16], respectively, and the three-body recombination rate constant L_3 for ^{85}Rb is about four orders of magnitude larger than for ^{87}Rb. Nevertheless, as a central result of our work, we find the spin propensity rule to also hold for ^{85}Rb, within the investigated range of binding energies from zero to $13\,\mathrm{GHz}\times h$ and the resolution of our experiment [17]. This result is corroborated by the fact that our measured product distributions are well reproduced by numerical three-body calculations based on a single-spin channel. The spin propensity rule that we find for ^{87}Rb and ^{85}Rb will also hold for other elements if certain conditions are met, which are formulated in the present work.

We carry out the measurements with an ultracold cloud of 2.5×10^5 ^{85}Rb ground state atoms at a temperature of 860 nK and at near-zero magnetic field B. The atoms have spin $f = 2, m_f = -2$ and are trapped in a far-detuned optical dipole trap [18]. Three-body recombination produces weakly-bound molecules in the mixed singlet $X^1\Sigma_g^+$ and triplet $a^3\Sigma_u^+$ states [see Fig. 1(a)], which are coupled by hyperfine interaction [16]. We measure the yields of molecular products, observing a range of rovibrational states with vibrational and rotational quantum numbers v, L_R, respectively, from $\mathrm{v} = -1$ to -4 [22] and from $L_R = 0$ to 6. A main result of our experiments is that we only find population in molecular states which are in the same spin state $F = 4, f_a = 2, f_b = 2$ (in short $Ff_af_b = 422$) as the reacting atom pair, although the investigated range of binding energies covers many bound states with different spin states. Because the two ^{85}Rb atoms (a,b) are identical bosons, the state $Ff_af_b = 422$ goes along with only having even angular momenta L_R and a positive total parity.

We have extended our previous state-selective detection scheme [8] so that it now covers all symmetries of the dimer product state space, including spin triplet and singlet states with their respective u/g symmetry. We apply two-step resonance-enhanced multiphoton ionization (REMPI), similar

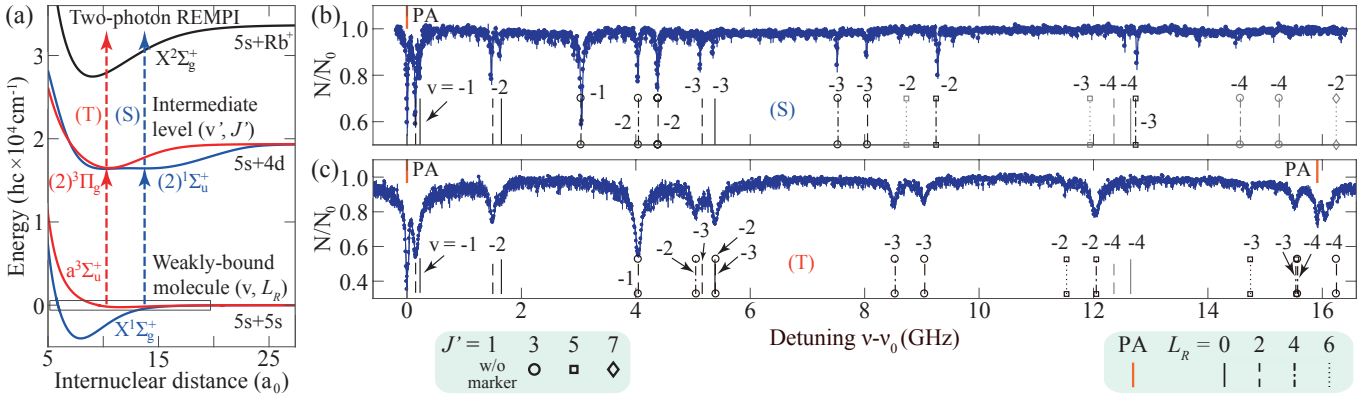

FIG. 1. (a) REMPI pathways for detecting molecules with singlet $X^1\Sigma_g^+$ and/or triplet $a^3\Sigma_u^+$ character via the intermediate states $(2)^1\Sigma_u^+$, $v' = 22$ [19] [path (S)] and $(2)^3\Pi_g, 0_g^+$, $v' = 10$ [19] [path (T)], respectively (see blue (red) dashed vertical arrows). The potential energy curves are derived from [16, 20, 21]. (b,c) REMPI spectra of product molecules using path (S) for (b) and path (T) for (c). Shown is the normalized remaining atom number N/N_0 as a function of the REMPI laser frequency ν, where $\nu_0 = 497603.591$ GHz (b), $\nu_0 = 497831.928$ GHz (c), are the resonance positions of the photoassociation signals (PA) of the intermediate levels with $J' = 1$. J' is the total angular momentum excluding nuclear spin. The vertical lines represent calculated resonance positions, where black (gray) color indicates experimentally observed (unobserved) states. Each line is marked with the vibrational quantum number v. L_R and J' are given by the linestyle and the plot symbols, respectively (see legends).

to [21, 23–26], but with a cw-laser. By two different REMPI pathways, (S) or (T), we probe product molecules via singlet or triplet character [see Fig. 1(a)]. Both schemes use identical photons for the two REMPI steps at wavelengths around 602.2 nm (see [18]). The intermediate states are deeply-bound levels of $(2)^1\Sigma_u^+$ and $(2)^3\Pi_g$ for REMPI (S) and (T), respectively. When ions are produced via REMPI, they are directly trapped and detected in an eV-deep Paul trap which is centered on the atom cloud. Subsequently, elastic atom-ion collisions inflict tell-tale atom loss while the ions remain trapped. From the atom loss which is measured via absorption imaging of the atom cloud [8, 27, 28] the ion number can be inferred [18].

Figures 1(b) and (c) show REMPI spectra of Rb_2 product molecules following three-body recombination, using path (S) and (T), respectively. Apart from three signals stemming from the photoassociation of two atoms (indicated by PA) [29], each resonance line of loss corresponds to a molecular product state. The photoassociation lines serve as references for the $|f = 2, m_f = -2\rangle + |f = 2, m_f = -2\rangle$ asymptote corresponding to zero binding energy at about zero magnetic field. The vertical lines in Figs. 1(b) and (c) are predicted frequency positions for product states for the spin state $Ff_af_b = 422$. These predictions are obtained from coupled-channel calculations for the $X^1\Sigma_g^+ - a^3\Sigma_u^+$ complex [16]. Coincidences of predicted and observed lines allow for an assignment. As a consistency check for the assignment of signals in Figs. 1(b) and (c) we make use of product states with $L_R > 0$ since these give rise to two resonance lines corresponding to the transitions towards $J' = L_R \pm 1$. Indeed, the data in Figs. 1(b) and (c) confirm this consistency. Inspection clearly shows, that all experimentally observed spectral lines in Figs. 1(b) and (c) can be explained as signals from product molecules with the spin $Ff_af_b = 422$. As an additional check for the line assignment, we show in [18] that our experimental spectra do not match up with molecular spin states other than $Ff_af_b = 422$. This clearly indicates that the same spin propensity rule previously observed for ^{87}Rb also holds for ^{85}Rb.

For each product signal in the singlet REMPI path (S) we obtain a corresponding signal in the triplet REMPI path (T). This is because the spin state $Ff_af_b = 422$, $m_F = -4$ has sizeable singlet ($\approx 15\%$) and triplet ($\approx 85\%$) admixtures. The spectra of Figs. 1(b) and (c) generally look different since the rotational constants differ for $(2)^1\Sigma_u^+$ ($B_{v'} = 289(1)$ MHz) and for $(2)^3\Pi_g, 0_g^+$ ($B_{v'} = 389(2)$ MHz), see, e.g., [30]. The linewidths in Fig. 1(c) are typically on the order of 100 MHz (FWHM) which is larger than the typical linewidths in Fig. 1(b) of about 30 MHz. This is a consequence of the larger hyperfine splitting of the $(2)^3\Pi_g$ state, which is not resolved in our measurements. In Fig. 1(c) at $\nu - \nu_0 = 15.90$ GHz there is a photoassociation signal which belongs to the 0_g^- component of $(2)^3\Pi_g$. We show the corresponding REMPI spectrum in [18]. It exhibits the same molecular states as in Figs. 1(b) and (c).

We now carry out a more quantitative analysis where we compare the experimental signal strengths of the various REMPI paths and also compare them to theoretical calculations. For this, we measure the ion production rate for each assigned resonance line in Fig. 1 and Fig. S1 [18]. For a given REMPI path, the ion rate signal is expected to be proportional to the product molecule population rate, if we assume equal REMPI ionization efficiencies for the states. Our data show that this assumption is indeed fulfilled for most data points within the uncertainty limits of the recordings.

Figure 2 shows the extracted ion production rates γ_i of each molecular product state for the three REMPI paths (via $(2)^1\Sigma_u^+$, $(2)^3\Pi_g\ 0_g^+$, and $(2)^3\Pi_g\ 0_g^-$). If a state is observed via

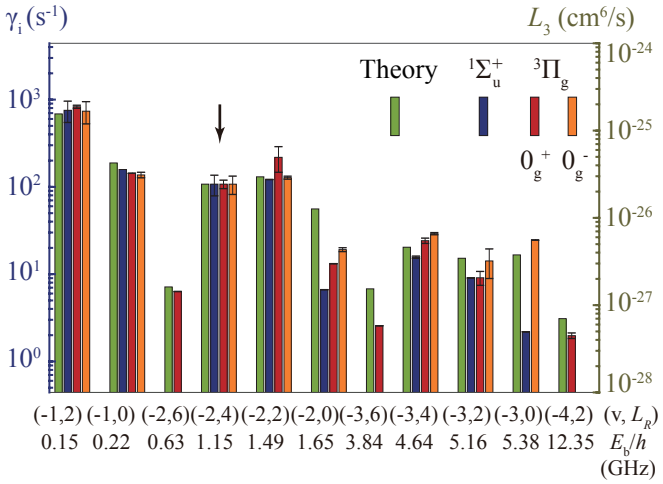

FIG. 2. Comparison of calculations and experiments. Measured (scaled) ion production rates γ_i for the product states (v, L_R) with binding energies E_b are given for the three REMPI paths together with calculations for the three-body recombination channel rate constants $L_3(\mathrm{v}, L_R)$ (see the legend for the color coding). The ion signals for the $(2)^3\Pi_g\ 0_g^-$ and $(2)^1\Sigma_u^+$ paths have been scaled (see text).

two or three different J' levels for a given path, we plot the average of the rates and mark the standard deviation from the mean with an error bar. In order to ease the comparison between the three data sets we have globally scaled the ion signals for the $(2)^3\Pi_g\ 0_g^-$ and $(2)^1\Sigma_u^+$ paths by a factor of 7.3 and 3.2, respectively, so that the signal bars for all REMPI paths in Fig. 2 are the same height for the state $(\mathrm{v}=-2,\ L_R=4)$, see black arrow. These scaling factors compensate the differences in the ionization efficiencies of the different REMPI paths, which are due to the different singlet and triplet components of the product molecule as well as differences in the electric dipole transition moments, which are generally not very well known yet [31]. After the scaling, the three distributions of the product rates are similar, indicating that for a given REMPI path the ionization efficiency is rather constant over the states.

In addition to the experimental data, we plot in Fig. 2 calculated channel rate constants $L_3(\mathrm{v}, L_R)$ for a temperature of $0.8\,\mu$K. The calculations use a single-spin model [18] which is similar to the one used in Ref. [8] in order to solve the three-body Schrödinger equation in an adiabatic hyperspherical representation [32, 33]. For this, we use pairwise additive long range van der Waals potentials with a scattering length of $-443\mathrm{a}_0$ [34] for ^{85}Rb and with a truncated number Z of $L_R=0$ bound states ($Z=9$ for Fig. 2). The calculated total recombination rate constant at $0.8\,\mu$K (including thermal averaging) is $L_3 = 3.07\times10^{-25}\ \mathrm{cm}^6/\mathrm{s}$ and is consistent with the values found in Ref. [35].

All data sets in Fig. 2 display the trend that the population of a molecular state due to three-body recombination typically decreases with increasing binding energy E_b of the product state, which is consistent with the work for ^{87}Rb [8]. The overall agreement between theory and experiment in Fig. 2 is good, as the experimentally observed relative strengths of the signals for low L_R are in general well reproduced by the calculated recombination rates. This suggests that our single-spin model fully captures the characteristics of the three-body chemical reaction in the given parameter regime, which can be viewed as additional evidence for the spin propensity rule.

Based on our theoretical analysis, we conclude that the observed spin propensity rule is a consequence of the following scenario. a) The reaction takes place at interparticle distances where the interactions of particles a and b (forming the molecule) with particle c are nearly spin-independent and therefore only mechanical. b) Within the investigated range of binding energies all possible molecular products have good quantum numbers F, f_a, f_b. c) In the reaction region, the spin composition of the reacting pair a,b is essentially given by $Ff_af_b = 422$. We will show below that [within the framework of condition a)] the conditions b) and c) hold when the splitting between neighboring triplet and singlet vibrational levels is much smaller than the atomic hyperfine splitting. As a consequence of conditions a), b) and c) the molecule formation is driven by mechanical forces from atom c while the spin state of the reacting pair is not affected.

To show that this scenario holds for our experiments, we first analyze the typical interparticle distances where the reaction occurs. Our numerical calculations [18] show that the formation of $^{85}\mathrm{Rb}_2$ molecules mainly takes place near a hyperradius $R \approx 1.5 r_{\mathrm{vdW}}$, extending from $R \approx 1.1 r_{\mathrm{vdW}}$ to $2r_{\mathrm{vdW}}$. Here, $r_{\mathrm{vdW}} = (2\mu C_6/\hbar^2)^{1/4} = 82a_0$ denotes the van der Waals length for Rb, and μ and C_6 are the reduced mass and the van der Waals coefficient of the two-particle system, respectively. The hyperradius R describes the characteristic size of the three-body system and is given by $R^2 = (\vec{r}_b-\vec{r}_a)^2/d^2 + d^2(\vec{r}_c-(\vec{r}_a+\vec{r}_b)/2)^2$, where $\vec{r}_i$ is the location of particle i and $d^2 = 2/\sqrt{3}$ [32]. The fact that the reactions occur at these large R can be understood within the framework of the adiabatic hyperspherical representation, where an effective repulsive barrier for the three-body entrance channel forms at a hyperradius of about $R = 1.7 r_{\mathrm{vdW}}$ [18, 36].

We now consider the formation of a molecule state with a size $\lesssim r_{\mathrm{hf}} \approx 0.6 r_{\mathrm{vdW}}$. Only for such a state can spin components other than $Ff_af_b = 422$ be substantial (for more details see [18]). Here, $r_{\mathrm{hf}} = (C_6/E_{\mathrm{hf}})^{1/6}$ is the hyperfine radius and $E_{\mathrm{hf}} = 3.04\,\mathrm{GHz}\times h$ is the atomic hyperfine splitting. Given the hyperradius $R > 1.1 r_{\mathrm{vdW}}$ and the interparticle distance $r_{ab} \equiv |\vec{r}_a - \vec{r}_b| < r_{\mathrm{hf}}$, the distances of particle c to the others must be $r_{ca}, r_{cb} > 0.6 r_{\mathrm{vdW}}$. Since the interaction between two Rb atoms is essentially spin-independent for distances larger than the spin-exchange distance $r_{\mathrm{ex}} = 0.25 r_{\mathrm{vdW}}$ (where the hyperfine splitting becomes larger than the spin-exchange interaction) [18], this validates point a) of the scenario described above. Concerning point b), our coupled-channel calculations show that the weakly-bound molecular states up to a binding energy of about $50\,\mathrm{GHz}\times h$ have almost pure spin states Ff_af_b. This can be explained by the fact that the ^{85}Rb triplet and singlet scattering lengths are large in magnitude. For ^{85}Rb, where these scattering lengths are of opposite sign,

this leads to a near energetical degeneracy of the triplet vibrational levels v_T with the singlet vibrational levels $v_S = v_T - 1$ [37, 38]. Since, in addition, the singlet and triplet vibrational wavefunctions are very similar at long range, the interaction between the two atoms is effectively spin-independent. As a consequence the atomic hyperfine interaction of each atom is essentially unperturbed, which leads to the atomic hyperfine structure with the quantum numbers f_a, f_b for the molecule. Subsequent coupling of $\vec{f}_a, \vec{f}_b$ in the molecule forms a total $\vec{F}$.

To show point c), we first note that due to the magnitude of R the three-body system can be effectively decomposed (with respect to spin) into a two-body collision of two $f = 2, m_f = -2$ atoms (a and b) and a third atom (c) which is spin-wise only a spectator, see also [18]. During the two-body collision of atoms a and b, spin admixtures to the original 422 state can occur at close distance. However, these admixtures are only on the % level for ^{85}Rb even for short atomic distances $r_{ij} \sim 0.25 r_{\mathrm{vdW}}$, and therefore negligible. That this admixture is small can be derived from the fact, that the two-body scattering wavefunction is very similar to the one of the corresponding last molecular bound state at short distance. The scattering state therefore shares the relatively pure $F f_a f_b$ spin state character of the weakly-bound molecular states, as discussed before.

Our coupled-channel calculations using the potentials of [16] show that for molecular bound states with a binding energy larger than $50\,\mathrm{GHz} \times h$ the spin decomposition changes, because the splitting of adjacent singlet and triplet vibrational levels becomes larger than the hyperfine splitting. This is shown in Fig. 3(a). In our experiment we only observe product states down to the $v = -4$ level in the 422 family, for which the norm of the 422 entrance channel remains between 0.99 and unity. All other unobserved spin families have a norm of the 422 channel much less than unity. In Fig. 3(b) we plot the ratio ρ of the triplet and singlet level splitting and the hyperfine splitting, $\rho = |E_{\mathrm{T}}(v) - E_{\mathrm{S}}(v-1)|/E_{\mathrm{hf}}$. Here, ρ is a main indicator for the conservation of the spin propensity rule, when considering weakly-bound states. For $\rho > 1$ hyperfine mixing of singlet and triplet states is increasingly suppressed and the propensity rule is expected to break down. For $\rho < 1$ the strong mixing of singlet and triplet states ensures that the product states are characterized by the spin family quantum numbers $F f_a f_b$, a central precondition for the propensity rule. Furthermore, when $\rho < 1$ the bond length of the product molecule is larger than r_{ex}. Since the bond length sets a typical length scale for the reaction distance, the reaction will likely take place at such large distances that interactions are purely mechanical.

A similar analysis as for ^{85}Rb atoms can be used to also explain the spin propensity rule for ^{87}Rb as observed in [8, 9]. Here, the singlet and triplet vibrational states for $v_T = v_S$ are nearly degenerate, as the singlet and triplet scattering lengths are almost equal. Furthermore, the atomic hyperfine splitting in ^{87}Rb is larger by a factor of ≈ 2.4 than in ^{85}Rb. As a consequence the spin propensity rule holds for even larger binding energies of up to $100\,\mathrm{GHz} \times h$ (see Fig S5 in [18]).

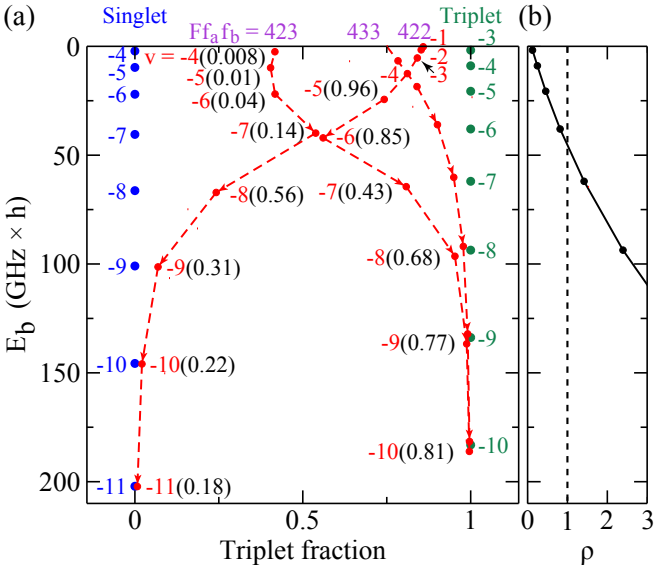

FIG. 3. (a) Binding energy and spin character of weakly-bound $^{85}Rb_2$ molecules for various vibrational quantum numbers $v = -1$ to -11 at $B = 0$ (red circles). Here, $L_R = 0$, $F = 4$, and $m_F = -4$. Zero energy corresponds to two separated atoms in state $f_a f_b = 22$. The spin character is given as the norm of the spin triplet component. Shown are the three spin families with $F = 4$ which correlate with the states $F f_a f_b = 422, 423, 433$ at the $E_b = 0$ threshold. Red dashed arrows are guides to the eye and indicate the change of each family's spin character with increasing binding energy. The norm of the 422 spin component is presented in parentheses for the 423 and 422 families. For the 433 family the 422 norm is about 1% for the shown bound states. Blue and green circles are the bound state levels of the pure singlet and triplet potentials, respectively, the dissociation limit of which is at $E = +3.542\,\mathrm{GHz} \times h$ above $E_b = 0$. (b) Ratio ρ for various binding energies (see text).

In the future, it will be interesting to investigate the breakdown of the spin propensity rule for ^{85}Rb by studying product molecules with binding energies larger than $\sim 50\,\mathrm{GHz} \times h$. For these measurements the ability to state-selectively detect singlet and triplet product molecules as demonstrated here, will be essential. The spin propensity rule will also break down when F is not a good quantum number anymore, e.g., by applying strong magnetic fields. ^{85}Rb features a broad Feshbach resonance at 153.3 G [39] where spin-mixing in the incoming channel naturally becomes important [11, 12, 40]. Besides for Rb the spin-conservation propensity rule may hold for other elements. Cs, e.g., might be a good candidate when working in a regime where dipolar relaxation processes are negligible.

This work was financed by the Baden-Württemberg Stiftung through the Internationale Spitzenforschung program (contract BWST ISF2017-061) and by the German Research Foundation (DFG, Deutsche Forschungsgemeinschaft) within contract 399903135. We acknowledge support from bwForCluster JUSTUS 2 for high performance computing. J. P. D. also acknowledges partial support from the U.S. National Science Foundation, Grant No. PHY-2012125, and NASA/JPL

1502690. The authors would like to thank Jinglun Li for helpful discussions. J. P. D. thanks Timur Tscherbul for stimulating discussions.

* shinsuke.haze@uni-ulm.de
† johannes.denschlag@uni-ulm.de

[1] R. S. Berry, Ionization of molecules at low energies, J. Chem. Phys. **45**, 1228 (1966).
[2] U. Fano, Propensity rules: An analytical approach, Phys. Rev. A **32**, 617 (1985).
[3] J. H. Moore, Investigation of the Wigner spin rule in collisions of N^+ with He, Ne, Ar, N_2, and O_2, Phys. Rev. A **8**, 2359 (1973).
[4] A. R. Lee, C. S. Enos, and A. G. Brenton, Collisional excitation of CO: a study of the Wigner spin rule, International Journal of Mass Spectrometry and Ion Processes **104**, 49 (1991).
[5] R. Hermsmeier, J. Kłos, S. Kotochigova, and T. V. Tscherbul, Quantum spin state selectivity and magnetic tuning of ultracold chemical reactions of triplet alkali-metal dimers with alkali-metal atoms, Phys. Rev. Lett. **127**, 103402 (2021).
[6] M.-G. Hu, Y. Liu, M. A. Nichols, L. Zhu, G. Quéméner, O. Dulieu, and K.-K. Ni, Nuclear spin conservation enables state-to-state control of ultracold molecular reactions, Nat. Chem. **13**, 435 (2021).
[7] Y. Liu, M.-G. Hu, M. A. Nichols, D. Yang, D. Xie, H. Guo, and K.-K. Ni, Precision test of statistical dynamics with state-to-state ultracold chemistry, Nature **593**, 379 (2021).
[8] J. Wolf, M. Deiß, A. Krükow, E. Tiemann, B. P. Ruzic, Y. Wang, J. P. D'Incao, P. S. Julienne, and J. Hecker Denschlag, State-to-state chemistry for three-body recombination in an ultracold rubidium gas, Science **358**, 921 (2017).
[9] J. Wolf, M. Deiß, and J. Hecker Denschlag, Hyperfine magnetic substate resolved state-to-state chemistry, Phys. Rev. Lett. **123**, 253401 (2019).
[10] J.-L. Li, T. Secker, P. M. A. Mestrom, and S. J. J. M. F. Kokkelmans, Strong spin-exchange recombination of three weakly interacting ^{7}Li atoms, arXiv:2107.11269 (2021).
[11] R. Chapurin, X. Xie, M. J. Van de Graaff, J. S. Popowski, J. P. D'Incao, P. S. Julienne, J. Ye, and E. A. Cornell, Precision test of the limits to universality in few-body physics, Phys. Rev. Lett. **123**, 233402 (2019).
[12] X. Xie, M. J. Van de Graaff, R. Chapurin, M. D. Frye, J. M. Hutson, J. P. D'Incao, P. S. Julienne, J. Ye, and E. A. Cornell, Observation of Efimov universality across a nonuniversal Feshbach resonance in ^{39}K, Phys. Rev. Lett. **125**, 243401 (2020).
[13] J. P. Burke, J. L. Bohn, B. D. Esry, and C. H. Greene, Impact of the ^{87}Rb singlet scattering length on suppressing inelastic collisions, Phys. Rev. A **55**, R2511 (1997).
[14] P. S. Julienne, F. H. Mies, E. Tiesinga, and C. J. Williams, Collisional stability of double Bose condensates, Phys. Rev. Lett. **78**, 1880 (1997).
[15] S. J. J. M. F. Kokkelmans, H. M. J. M. Boesten, and B. J. Verhaar, Role of collisions in creation of overlapping Bose condensates, Phys. Rev. A **55**, R1589 (1997).
[16] C. Strauss, T. Takekoshi, F. Lang, K. Winkler, R. Grimm, J. Hecker Denschlag, and E. Tiemann, Hyperfine, rotational, and vibrational structure of the $a^3\Sigma_u^+$ state of $^{87}Rb_2$, Phys. Rev. A **82**, 052514 (2010).
[17] While we do not resolve the molecular m_F quantum number in the present work, the conservation of m_F should hold judging from our previous work on ^{87}Rb [9] and our insights gained in the present work.
[18] See Supplementary Material at ..., which includes Refs. [41–44] for further information about the experimental setup and methodology, the theoretical model, additional REMPI data, as well as aspects and tests of the spin propensity rule.
[19] M. Ascoli, Spectroscopy of states with ion-pair character near Rb(5s)+Rb(4d), Doctoral Dissertation, University of Connecticut (2015).
[20] M. A. Bellos, R. Carollo, J. Banerjee, M. Ascoli, A.-R. Allouche, E. E. Eyler, P. L. Gould, and W. C. Stwalley, Upper bound to the ionization energy of $^{85}Rb_2$, Phys. Rev. A **87**, 012508 (2013).
[21] J. Lozeille, A. Fioretti, C. Gabbanini, Y. Huang, H. K. Pechkis, D. Wang, P. L. Gould, E. E. Eyler, W. C. Stwalley, M. Aymar, and O. Dulieu, Detection by two-photon ionization and magnetic trapping of cold Rb_2 triplet state molecules, Eur. Phys. J. D **39**, 261 (2006).
[22] Here, v is counted downwards, starting with -1 for the last s-wave bound state just below the atom pair asymptote $|f=2,m_f=-2\rangle+|f=2,m_f=-2\rangle$.
[23] Y. Huang, J. Qi, H. K. Pechkis, D. Wang, E. E. Eyler, P. L. Gould, and W. C. Stwalley, Formation, detection and spectroscopy of ultracold Rb_2 in the $X^1\Sigma_g^+$ state, J. Phys. B: At. Mol. Opt. Phys. **39**, S857 (2006).
[24] C. Gabbanini, A. Fioretti, A. Lucchesini, S. Gozzini, and M. Mazzoni, Cold rubidium molecules formed in a magneto-optical trap, Phys. Rev. Lett. **84**, 2814 (2000).
[25] S. Jyothi, T. Ray, S. Dutta, A. R. Allouche, R. Vexiau, O. Dulieu, and S. A. Rangwala, Photodissociation of trapped Rb_2^+: Implications for simultaneous trapping of atoms and molecular ions, Phys. Rev. Lett. **117**, 213002 (2016).
[26] M. W. Mancini, G. D. Telles, A. R. L. Caires, V. S. Bagnato, and L. G. Marcassa, Observation of ultracold ground-state heteronuclear molecules, Phys. Rev. Lett. **92**, 133203 (2004).
[27] A. Härter, A. Krükow, A. Brunner, and J. Hecker Denschlag, Minimization of ion micromotion using ultracold atomic probes, Appl. Phys. Lett. **102**, 221115 (2013).
[28] A. Härter, A. Krükow, M. Deiß, B. Drews, E. Tiemann, and J. Hecker Denschlag, Population distribution of product states following three-body recombination in an ultracold atomic gas, Nat. Phys. **9**, 512 (2013).
[29] K. M. Jones, E. Tiesinga, P. D. Lett, and P. S. Julienne, Ultracold photoassociation spectroscopy: Long-range molecules and atomic scattering, Rev. Mod. Phys. **78**, 483 (2006).
[30] Y. Guan, X. Han, J. Yang, Z. Zhou, X. Dai, E. H. Ahmed, A. M. Lyyra, S. Magnier, V. S. Ivanov, A. S. Skublov, and V. B. Sovkov, Updated potential energy function of the Rb_2 $a^3\Sigma_u^+$ state in the attractive and repulsive regions determined from its joint analysis with the $2^3\Pi_{0g}$ state, J. Chem. Phys. **139**, 144303 (2013).
[31] We note that because of these uncertainties and uncertainties in the atom number calibration we refrain from converting the measured ion production rates into three-body recombination rate constants for each product channel.
[32] J. P. D'Incao, Few-body physics in resonantly interacting ultracold quantum gases, J. Phys. B: At. Mol. Opt. Phys. **51**, 043001 (2018).
[33] J. Wang, J. P. D'Incao, and C. H. Greene, Numerical study of three-body recombination for systems with many bound states, Phys. Rev. A **84**, 052721 (2011).
[34] N. R. Claussen, S. J. J. M. F. Kokkelmans, S. T. Thompson, E. A. Donley, E. Hodby, and C. E. Wieman, Very-high-precision bound-state spectroscopy near a ^{85}Rb Feshbach reso-

nance, Phys. Rev. A **67**, 060701 (2003).

[35] J. L. Roberts, N. R. Claussen, S. L. Cornish, and C. E. Wieman, Magnetic field dependence of ultracold inelastic collisions near a Feshbach resonance, Phys. Rev. Lett. **85**, 728 (2000).

[36] J. Wang, J. P. D'Incao, B. D. Esry, and C. H. Greene, Origin of the three-body parameter universality in Efimov physics, Phys. Rev. Lett. **108**, 263001 (2012).

[37] P. S. Julienne, Ultracold molecules from ultracold atoms: a case study with the KRb molecule, Faraday Discuss. **142**, 361 (2009).

[38] P. S. Julienne, Molecular states near a collision threshold, Chap. 6 in *Cold Molecules: Theory, Experiment, Applications*, edited by R. Krems, B. Friedrich, and W. C. Stwalley, CRC press (2009).

[39] C. L. Blackley, C. R. Le Sueur, J. M. Hutson, D. J. McCarron, M. P. Köppinger, H.-W. Cho, D. L. Jenkin, and S. L. Cornish, Feshbach resonances in ultracold ^{85}Rb, Phys. Rev. A **87**, 033611 (2013).

[40] T. Secker, J.-L. Li, P. M. A. Mestrom, and S. J. J. M. F. Kokkelmans, Multichannel nature of three-body recombination for ultracold ^{39}K, Phys. Rev. A **103**, 022825 (2021).

[41] A. Mohammadi, A. Krükow, A. Mahdian, M. Deiß, J. Pérez-Ríos, H. da Silva, M. Raoult, O. Dulieu, and J. Hecker Denschlag, Life and death of a cold $BaRb^+$ molecule inside an ultracold cloud of Rb atoms, Phys. Rev. Research **3**, 013196 (2021).

[42] J. P. D'Incao and B. D. Esry, Manifestations of the Efimov effect for three identical bosons, Phys. Rev. A **72**, 032710 (2005).

[43] G. Pichler, S. Milošević, D. Veža, and R. Beuc, Diffuse bands in the visible absorption spectra of dense alkali vapours, J. Phys. B: Atom. Mol. Phys. **16**, 4619 (1983).

[44] T. Köhler, K. Góral, and P. S. Julienne, Production of cold molecules via magnetically tunable Feshbach resonances, Rev. Mod. Phys. **78**, 1311 (2006).